Int. J. Radiation Oncology Biol. Phys., Vol. 53, No. 4, pp. 822–834, 2002

0360-3016/02/$–see front matter

ELSEVIER

PII S0360-3016(02)02803-1

CLINICAL INVESTIGATION **Lung**

PRECISE AND REAL-TIME MEASUREMENT OF 3D TUMOR MOTION IN LUNG DUE TO BREATHING AND HEARTBEAT, MEASURED DURING RADIOTHERAPY

YVETTE SEPPENWOOLDE, M.SC.,* HIROKI SHIRATO, M.D., PH.D.,† KEI KITAMURA, M.D., PH.D.,† SHINICHI SHIMIZU, M.D., PH.D.,† MARCEL VAN HERK, PH.D.,* JOOS V. LEBESQUE, M.D., PH.D.,* AND KAZUO MIYASAKA, M.D., PH.D.†

*Department of Radiotherapy, The Netherlands Cancer Institute, Antoni van Leeuwenhoek Hospital, Amsterdam, The Netherlands; †Department of Radiation Medicine, Hokkaido University School of Medicine, Sapporo, Japan

Purpose: In this work, three-dimensional (3D) motion of lung tumors during radiotherapy in real time was investigated. Understanding the behavior of tumor motion in lung tissue to model tumor movement is necessary for accurate (gated or breath-hold) radiotherapy or CT scanning.

Methods: Twenty patients were included in this study. Before treatment, a 2-mm gold marker was implanted in or near the tumor. A real-time tumor tracking system using two fluoroscopy image processor units was installed in the treatment room. The 3D position of the implanted gold marker was determined by using real-time pattern recognition and a calibrated projection geometry. The linear accelerator was triggered to irradiate the tumor only when the gold marker was located within a certain volume. The system provided the coordinates of the gold marker during beam-on and beam-off time in all directions simultaneously, at a sample rate of 30 images per second. The recorded tumor motion was analyzed in terms of the amplitude and curvature of the tumor motion in three directions, the differences in breathing level during treatment, hysteresis (the difference between the inhalation and exhalation trajectory of the tumor), and the amplitude of tumor motion induced by cardiac motion.

Results: The average amplitude of the tumor motion was greatest (12 ± 2 mm [SD]) in the cranial-caudal direction for tumors situated in the lower lobes and not attached to rigid structures such as the chest wall or vertebrae. For the lateral and anterior-posterior directions, tumor motion was small both for upper- and lower-lobe tumors (2 ± 1 mm). The time-averaged tumor position was closer to the exhale position, because the tumor spent more time in the exhalation than in the inhalation phase. The tumor motion was modeled as a sinusoidal movement with varying asymmetry. The tumor position in the exhale phase was more stable than the tumor position in the inhale phase during individual treatment fields. However, in many patients, shifts in the exhale tumor position were observed intra- and interfractionally. These shifts are the result of patient relaxation, gravity (posterior direction), setup errors, and/or patient movement.

The 3D trajectory of the tumor showed hysteresis for 10 of the 21 tumors, which ranged from 1 to 5 mm. The extent of hysteresis and the amplitude of the tumor motion remained fairly constant during the entire treatment. Changes in shape of the trajectory of the tumor were observed between subsequent treatment days for only one patient. Fourier analysis revealed that for 7 of the 21 tumors, a measurable motion in the range 1–4 mm was caused by the cardiac beat. These tumors were located near the heart or attached to the aortic arch. The motion due to the heartbeat was greatest in the lateral direction. Tumor motion due to hysteresis and heartbeat can lower treatment efficiency in real-time tumor tracking–gated treatments or lead to a geographic miss in conventional or active breathing controlled treatments.

Conclusion: The real-time tumor tracking system measured the tumor position in all three directions simultaneously, at a sampling rate that enabled detection of tumor motion due to heartbeat as well as hysteresis. Tumor motion and hysteresis could be modeled with an asymmetric function with varying asymmetry. Tumor motion due to breathing was greatest in the cranial-caudal direction for lower-lobe unfixed tumors. **© 2002 Elsevier Science Inc.**

Respiratory movement, Lung, Radiotherapy, Heartbeat.

INTRODUCTION

Recent developments in radiotherapy such as intensity-modulated radiotherapy, noncoplanar conformal radiotherapy (1–5), and active breathing controlled–gated treatments (6) are all aimed at increasing the tumor dose and reducing the dose to normal tissue. Discrepancies in tumor position between treatment and a planning computed tomography

Reprint requests to: Hiroki Shirato, M.D., Department of Radiation Medicine, Hokkaido University School of Medicine, North-15 West-7, Sapporo, Japan. E-mail: hshirato@radi.med.hokudai.ac.jp

Received Aug 21, 2001, and in revised form Feb 25, 2002. Accepted for publication Mar 4, 2002.

Table 1. Patient characteristics

Patient no.	Age	KI*	Pathology	Marker location	T stage	Dose (Gy)	Tumor size (cm^3)
1	77	70	Squamous cell	Near	2	40	14
2	52	80	Squamous cell	Near	1	35	85
3	72	80	Squamous cell	In	4	40	22
4	70	80	Adenocarcinoma	Near	2	40	20
5	70	50	Squamous cell	In	3	40	10
6	72	80	Squamous cell	In	3	40	36
7	77	70	Squamous cell	Near	1	40	60
8	76	70	Adenocarcinoma	In	1	40	16
9a	83	80	Squamous cell	Near	1	40	10
9b			Adenocarcinoma	Near	1	40	14
10	43	90	Adenocystic carcinoma, metastatic	Near	–	40	8
11	69	90	Squamous cell	In	2	35	192
12	55	70	Adenocarcinoma	Near	2	35	3
13	68	40	Squamous cell	Near	2	40	135
14	57	70	Squamous cell, metastatic	In	–	35	23
15	84	80	Squamous cell	Near	1	40	14
16	41	80	Renal cell carcinoma, metastatic	In	–	40	168
17	81	80	Adenocarcinoma	In	3	35	257
18	67	90	Bronchioalveolar	In	3	35	2
19	81	80	Adenocarcinoma	Near	2	40	9
20	70	90	Squamous cell	In	1	40	25

*Karnofsky index.

(CT) scan can be caused by setup errors and organ motion (7–9). To account for these errors, a safety margin is added to the clinical target volume to obtain the planning target volume. Reducing setup error and understanding organ motion are essential in designing the tightest possible safety margin without compromising the tumor coverage. To examine the motion of lung tumors during respiration, Ekberg *et al.* (10) used fluoroscopy at the time of simulation. They demonstrated an average movement of 3.9 mm (range: 0–12 mm) in the cranial-caudal direction, 2.4 mm (range: 0–5 mm) in the mediolateral direction, and 2.4 mm (range: 0–5 mm) in the dorsoventral direction. Breath-hold (6, 11) or gated (12, 13) radiotherapy is designed to reduce tumor motion due to breathing. A novel method of accurate dose delivery to moving tumors with small margins is the real-time tumor tracking radiotherapy (RTRT) system (14–16).

Three-dimensional (3D) treatment planning is often performed on a CT scan made while the patient breathes freely, under the assumption that the CT image represents the average position of the tumor. However, breathing motion can cause misdetection of the tumor during CT scanning, especially for small tumors, resulting in a smaller planning volume or a distorted tumor shape (17). To obtain an accurate tumor image, a breath-hold CT is preferable. The ideal breathing phase in which the breath-hold CT is taken must correspond to the average tumor position. When the breathing motion of the tumor is not symmetric, the average tumor location is no longer midway between the inhale and exhale tumor position.

In this study, precise 3D recordings of tumor position were made during RTRT treatment, both beam-on *and* beam-off periods, at a high sampling rate to determine and model tumor motion due to breathing, heartbeat, and patient motion.

PATIENTS AND METHODS

Twenty patients with tumors at different sites in the lung (One patient had two tumors) were included in the analysis (Table 1). Seventeen patients had non–small-cell primary lung cancer, and three had metastatic lung tumors. A typical treatment schedule consisted of 4×10 Gy with a four-field noncoplanar conformal technique using multiple static beams (4 MV) shaped with a multileaf collimator.

A 2.0-mm gold marker was implanted into or near the tumor mass using bronchial endoscopy or, when the tumor was situated near the thoracic wall, percutaneous needle insertion. Free-breathing CT scans were taken of the entire lung volume using a 5-mm slice thickness and a 5-mm slice interval. At the level of the tumor and the inserted marker, the slice thickness and slice interval were 1 mm or, if the tumor was large, 3 mm. Additionally, voluntary breath-hold CT scans were made at the inhalation and exhalation phases of tidal breathing, with the same slice thickness as for the free-breathing scan. A physician delineated the gold marker and the clinical target volume in each slice, and the position of the marker relative to the tumor was determined. Of the three CT scans, the scan that yielded the best possibility for irradiating the tumor (concerning normal tissue damage, tumor coverage, and treatment efficiency) was chosen as the planning CT scan. Three-dimensional treatment planning was performed using the Focus system (CMS, St. Louis, MO).

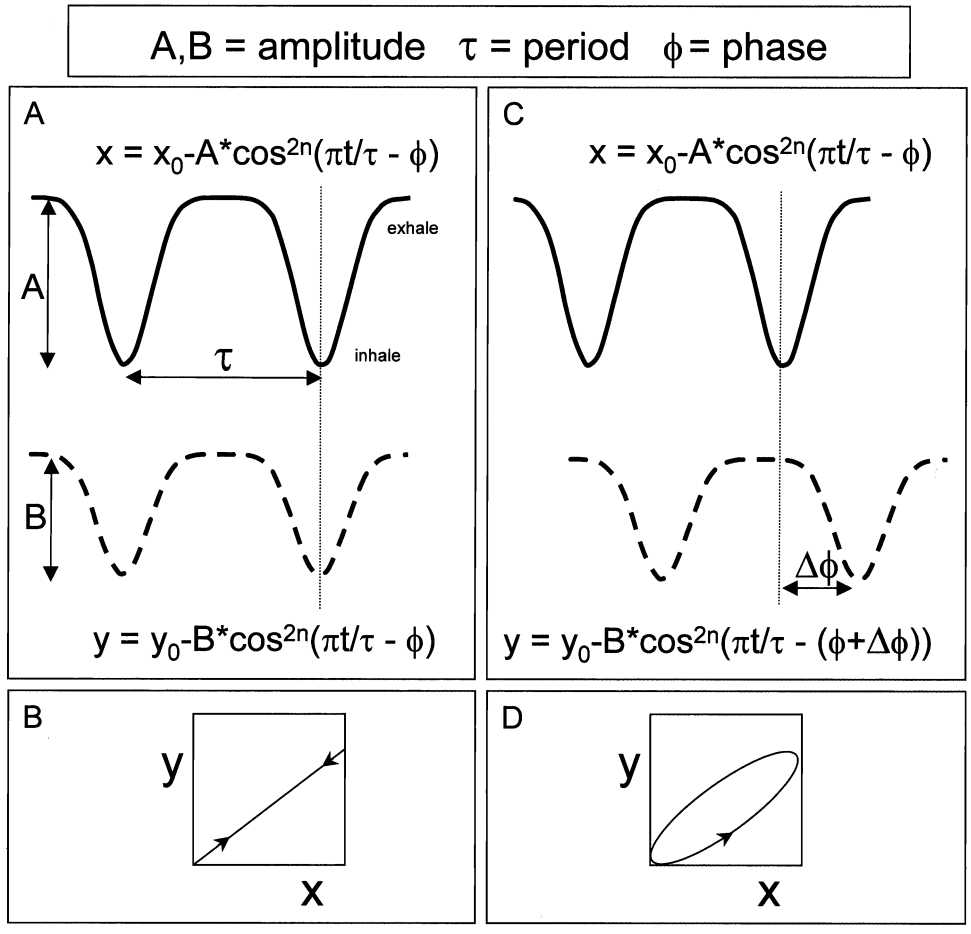

Fig. 1. The principle of hysteresis. When there is (A) no phase difference between two sinusoid signals with equal frequency, there is (B) no hysteresis; the position of the *y* direction is directly related to that of the *x* direction. When there is (C) a phase difference (ϕ), there are two possible positions where the tumor is at the same *x* position, depending on (D) the position in the breathing cycle. (D) The width and the shape of the hysteresis ellipsoid depend on the phase difference and the amplitude of both signals.

The fluoroscopic real-time tumor tracking radiotherapy system consists of four sets of diagnostic fluoroscopy, image processor units, a trigger control unit, an image display unit, and a conventional linear accelerator with multileaf collimators (15). Using two of the four fluoroscopy image processor units, the system determines the 3D position of the gold marker 30 times a second by using real-time pattern recognition and calibrated projection geometry. To avoid the blocking of the fluoroscopic images by the gantry of the linear accelerator, any two of the four X-ray systems may be selected. During the setup stage of each treatment fraction, the patient is positioned with skin markers. The physician judges both tumor position and motion based on two fluoroscopy images. The position of the treatment couch is adjusted when the gold marker is not found within the planned region. The zero tumor position is set by the physician at the position that best corresponds to the intended treatment breathing phase, based on the planning CT (In most cases, this was the exhale phase). Because the placement of the zero position may differ slightly from day to day, the error made in this position is described as the "residual setup error".

During treatment, the linear accelerator was triggered to irradiate the tumor only when the gold marker was located within a specified region of the planned coordinates relative to the isocenter. The delay between recognition of the marker and the start of irradiation was 0.09 s. Radiation oncologists defined the distance of the permitted dislocation of the tumor in the lateral (LR), cranial-caudal (CC), and ventral-dorsal (AP) directions, resulting in a box around the isocenter. The permitted displacement for each patient was typically $3 \times 3 \times 3$ mm^3.

The LR, CC, and AP coordinates of the internal marker were recorded 30 times per second during the treatment. Analog video images of the two fluoroscopic images were recorded simultaneously. All available data sets (each fraction and each beam direction) were analyzed for each patient; on average, there were 16 sets of 300 s per patient. The raw data of the RTRT system were filtered with a 30-point median filter to reduce system

Table 2. The mean amplitude of tumor motion, related to tumor location and attachment, the value of *n* for the fitted breathing curve, and the length of the breathing period

Patient no.	Mean amplitude* (mm ± 1 SD) LR	CC	AP	Lobe	Tumor attached to:	*n*	Breathing period (s ± 1 SD)
20	1.8 (0.4)	24.6 (3.8)	1.9 (0.4)	Lower		1	3.8 (0.6)
9a	1 (0.3)	13.1 (2.7)	3.6 (0.5)	Lower		2	3.6 (0.4)
10	1.4 (0.3)	11.8 (0.9)	2.6 (0.5)	Lower		1–2	4 (0.3)
3	0.5 (0.4)	10 (0.8)	1.7 (0.5)	Lower		2	3 (0.3)
7	2.5 (0.3)	7.7 (0.9)	0.9 (0.1)	Lower	Aorta	2	3.3 (0.8)
18	2 (0.4)	5.4 (1.0)	0.9 (0.2)	Lower		3–9	6.6 (1.5)
17	0.4 (0.1)	1 (0.3)	1.7 (0.5)	Lower	Anterior chest wall	1	3.8 (0.6)
16	0.5 (0.1)	0.2 (0.1)	0.2 (0.1)	Lower	Posterior chest wall	1	4.9 (0.8)
19	1.1 (0.3)	11.1 (2)	5.8 (0.7)	Middle		2	3.2 (0.3)
6	0.2 (0.1)	0.7 (0.1)	1.2 (0.1)	Middle	Lateral chest wall	2	4.8 (0.5)
8	0.6 (0.1)	8.7 (0.8)	8.2 (0.5)	Upper		2–3	3.8 (0.3)
12	1.3 (0.2)	4.2 (0.6)	4.1 (0.5)	Upper		2	3.2 (0.4)
9b	2.8 (0.6)	3 (0.5)	2.5 (0.5)	Upper	Vertebra and aortic arch	1	3.5 (0.3)
1	2.8 (0.3)	2.8 (0.4)	1.5 (0.2)	Upper		2	2.8 (0.2)
5	0.4 (0.1)	2.8 (0.6)	0.8 (0.3)	Upper	Bronchial	2	2.7 (0.4)
11	1.7 (0.3)	2.5 (0.4)	1.4 (0.2)	Upper	Aorta	1	3.2 (0.4)
15	0.7 (0.1)	2 (0.4)	2.7 (0.2)	Upper		1	3.2 (0.3)
14	0.6 (0.1)	1.5 (0.2)	1.4 (0.2)	Upper		1–2	3.7 (0.4)
4	0.6 (0.1)	1.2 (0.2)	2 (0.4)	Upper	Lateral chest wall	1	3.2 (0.4)
2	2.4 (0.4)	1 (0.2)	1.2 (0.1)	Upper	Aorta	1	3.3 (0.3)
13	0.5 (0.1)	0.7 (0.1)	0.6 (0.1)	Upper	Aortic arch	1	3.7 (0.5)

*Tumor motion of more than 5 mm is underlined.

noise. For each data set, the individual breathing cycles were detected automatically by thresholding, after inconsistent readings of the inferred position of the marker were manually removed. These inconsistent readings occurred during about 1% of the treatment time, depending on the visibility of the gold marker on the fluoroscopic images. Different parameters were measured during the individual breathing cycles: the amplitude, the position of the tumor in the inhale and exhale phases, the average tumor position, and the length of the breathing cycle. All the individual breathing cycles recorded during one beam direction were averaged.

The position *s* of the tumor as a function of time *t* can be defined as follows (18):

$$s(t) = s_0 - S\cos^{2n}(\pi t/\tau - \phi) \quad (1)$$

where s_0 is the position of the tumor at exhalation, S is the amplitude, and hence $s_0 - S$ is the position at inhalation; τ is the period of the breathing cycle in seconds, and ϕ is the starting phase. This parameterized breathing curve was fitted (using a least-squares method) through each average breathing cycle. Hysteresis was assessed by the phase difference in the average breathing curves from two directions (Fig. 1). The amount of clinically relevant hysteresis was determined as the maximum distance between the different trajectories that the tumor followed during inhalation and exhalation.

To separate tumor motion caused by heartbeat and breathing, the discrete Fourier transform of the unfiltered data were determined, resulting in the power spectrum of the signal. Fourier analysis breaks down a signal into constituent sinusoids of different frequencies. The power of a certain frequency represents the strength of this frequency in the time signal. Typical breathing in this data set has a frequency 0.2–0.3 Hz (a 3–5-s cycle). The heart beats with a frequency of around 1 Hz (60 bpm). The breathing frequency and the cardiac frequency do not overlap. When a peak of around 1 Hz was detected in the order of the power of the breathing signal, the raw signal was filtered with different settings (a high-pass digital filter with a cutoff of 0.5 Hz to eliminate the breathing frequency) to determine the amplitude of the motion due to heartbeat in all three directions.

RESULTS

Amplitude

For each patient, the average amplitude of the tumor motion was assessed in all three directions (Table 2). In the cranial-caudal (*y*) direction, tumors situated in the lower lobes and not attached to rigid structures, such as the chest wall or vertebrae, move more than upper-lobe tumors or tumors attached to rigid structures: 12 ± 6 and 2 ± 2 mm (SD), respectively, ($p = 0.005$, two-tailed, unequal variances). For tumors attached to rigid structures and for the LR and AP directions, there was no difference in amplitude between upper- and lower-lobe tumors; the motion was small in these directions: 1.2 ± 0.9 mm (SD) for the LR direction and 2.2 ± 1.9 mm (SD) for the AP direction. Two patients showed tumor motion

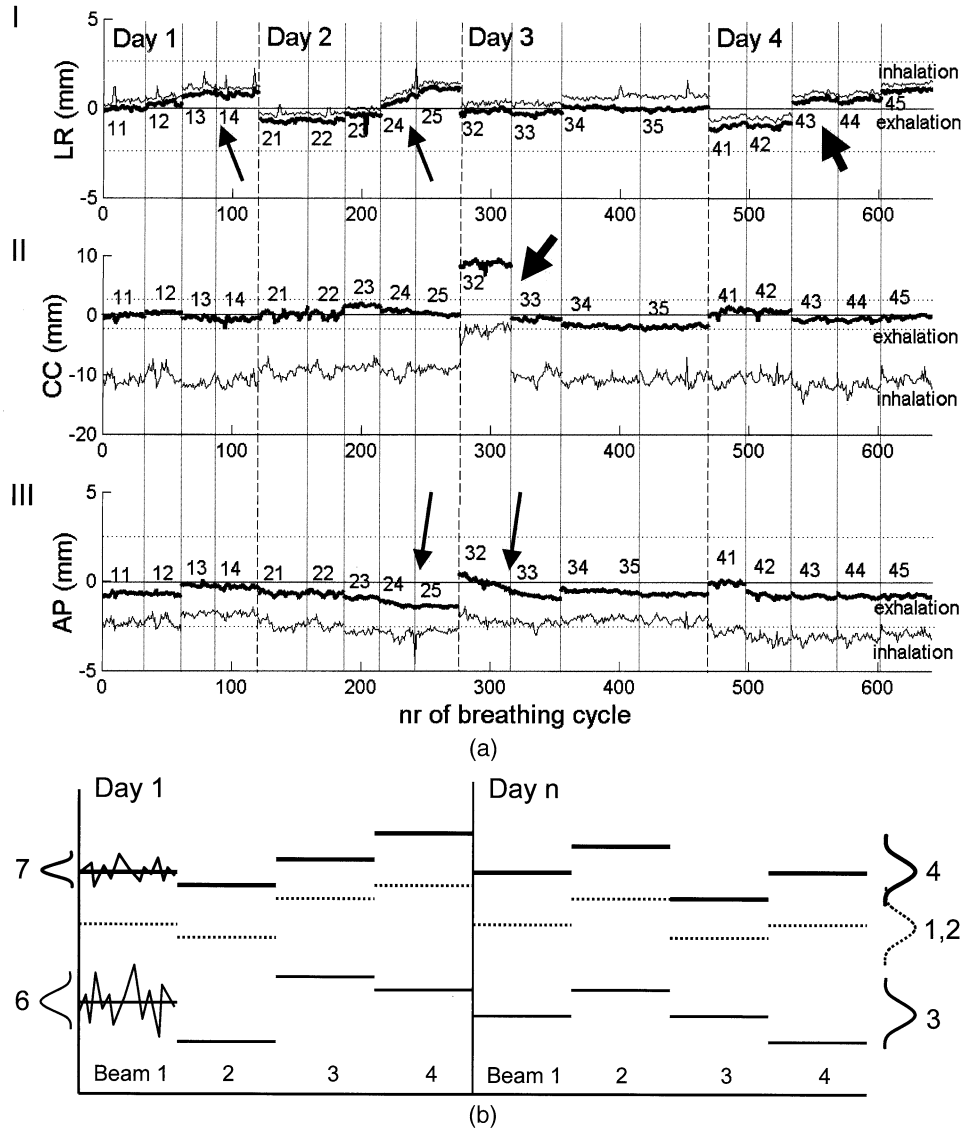

Fig. 2. (a) Position of inhalation and exhalation phase of Patient 3 during the treatment: I, LR direction; II, CC direction; and III, AP direction. The numbers represent the days and the beam directions; for example, 21 is the first beam on Day 2. The variation in the inhale position is larger than in the exhale position. Between the days and between the beams, a systematic shift in the average tumor position can be present (thick arrow). In the AP and LR directions, a gradual shift is present in the course of one treatment day (thin arrows). (The treatment efficiency of beam 15 and beam 31 was too low, and this beam was delivered without using the RTRT system with a larger margin.) (b) The different variations in tumor position that were given in Table 3 (The numbers in the figure correspond to the numbers used in Table 3) are as follows: (*1*) The average tumor position represents the difference between the planned zero-position and the actual tumor position during the treatment averaged over all patients. The systematic deviation from 0 is because the planned zero-position was normally the exhale and not the average tumor position. (*2*) The variation in the average tumor position contains variation in residual setup errors, breathing, patient movement during and between treatment days, and changes in breathing level and intensity. (*3*) The variation in the average inhale tumor position contains variation in residual setup errors, breathing, patient movement during and between treatment days, and changes in breathing level and intensity. (*4*) The variation in the average exhale tumor position, variation in residual setup errors, breathing, patient movement during and between treatment days, and changes in breathing level. (*6*) The variation in the inhale tumor position, corrected for its average, contains variation in patient movement *during* treatment, and changes in breathing level and intensity. (*7*) The variation in the exhale tumor position, corrected for its average, contains variation in patient movement *during* treatment and changes in breathing level.

of more than 5 mm in the AP direction; both tumors were located anterior and in the middle of the thorax (Patients 8 and 19). The average efficiency (total treatment time/ total irradiation time) of the RTRT system is 59% for this patient group. The efficiency depends on the amplitude of the breathing motion and the size of the box representing the permitted displacement. When the tumor motion was large, the relative amount of time that the tumor spent

outside the permitted displacement region was large, and the treatment efficiency was low. When the treatment efficiency dropped below 10%, the RTRT treatment was abandoned, and the patient was treated using a conventional treatment technique.

Average tumor position

Six patients showed a time trend in tumor position during one beam direction or during one treatment day, mostly in the posterior direction. Between the beams, shifts in the tumor position were frequently observed in all three directions (for example, Patient 3 [Fig. 2A]). Between subsequent days, the average tumor position could also shift. The trends and the shifts during one treatment day may have been caused by patient motion or internal tumor motion (change in breathing level), whereas for the shifts between subsequent days, the "residual setup error" would have played a role, as well.

The average tumor position and the variations in average tumor position, amplitude, and inhale and exhale tumor positions, averaged for each treatment beam or corrected for its average (Fig. 2B), are given in Table 3. The variations in the averages of the exhale and inhale tumor positions were comparable to the corresponding values of the average tumor position.

For the CC and AP directions, the variation in the inhale and exhale tumor positions, corrected for the average values (and thus corrected for the shifts between the beams and between the days), was smaller (p value $<$ 0.001, paired t test) than the variation in the inhale position.

3D path of the tumor

Visualization of the 3D path of the tumor (Fig. 3A) gave an impression of the hysteresis and the relation of the tumor motion to the permitted displacement (gate range). The shape of the average 3D curve (Fig. 3B) was fairly constant in time; differences were mainly because of shifts in average tumor position and changes in amplitude. The projections of the trajectories of the tumors on the coronal and sagittal plane were calculated for each patient (Fig. 4). The tumors attached to rigid structures are encircled. A change in the shape of the 3D path was observed between subsequent days in only 1 patient (Fig. 5).

Table 3. Summary statistics of tumor positions (in mm): see also Fig. 2B

	LR	CC	AP
1. Average tumor position	−0.4	−1.5	−1.6
2. SD in average tumor position	0.8	1.2	1.1
3. SD in average inhale tumor position	0.9	1.3	1.1
4. SD in average exhale tumor position	0.8	1.2	1.1
5. SD in amplitude	0.2	0.8	0.3
6. SD in inhale tumor position*	0.2	0.8	0.4
7. SD in exhale tumor position*	0.2	0.4	0.3

Abbreviations: SD = standard deviation; LR = lateral; CC = cranial-caudal; AP = ventral-dorsal.

*Corrected for changes in average ex- or inhale position.

Shape and length of the breathing cycle

For the patient group in this study, the average length of one breathing cycle was 3.6 ± 0.8 s (SD). The individual breathing periods and the variation during treatment are given in Table 2.

For each patient, the parameters of the sinusoid (Eq. 1) were determined. Equation 1 fitted well for the majority of the patients (Fig. 6A); the fitted values for the amplitude and

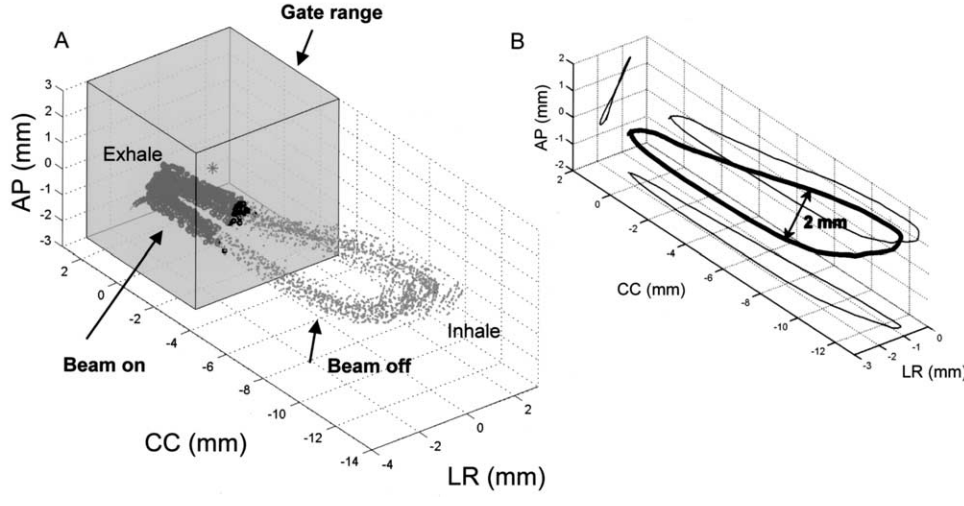

Fig. 3. (A) The 3D path of the tumor of Patient 10 during one treatment portal: The gray dots represent the tumor position throughout the treatment, and the black dots represent the tumor position as the tumor is detected to be inside the RTRT range (transparent box). The asterisk represents the planned zero position. (B) The average 3D curve of the tumor: The projections on the coronal, sagittal, and axial planes are drawn in thin black lines. Note that the tumor follows a different path during inhalation than during exhalation (hysteresis).

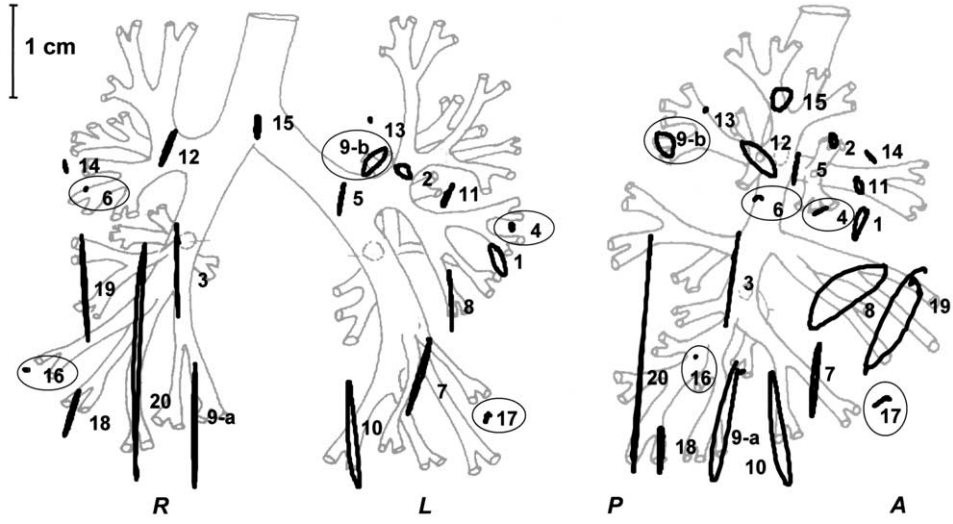

Fig. 4. Orthogonal projections of the trajectories of the 21 tumors on (left) the coronal (LR-CC) and (right) the sagittal (AP-CC) plane. The tumors are displayed at the approximate position, based on the localization mentioned in the treatment chart. Tumors that were attached to bony structures are circled.

period agreed with the measured values. The value for n varied between patients (Table 2). For 2 patients, the parameters $n = 1$ and $n = 2$ fitted equally well, suggesting that the shape of the actual breathing curve was somewhere between the two parameterized curves. In one case, the patient's breathing was very irregular, and the value for n varied between 3 and 9 (Fig. 6B), depending on the breathing period—the longer the period, the higher the value of n. However, the shape of the tumor motion for the longer period was similar to that of the shorter cycle; only the time spent in the exhale position was prolonged in the longer cycle. The value of n did not correlate with the breathing period for the whole patient group.

Hysteresis

In the (average) trajectories of the tumor, hysteresis was observed in 10 of the 20 patients: The tumor followed a different path during inhalation than during exhalation. The presence of hysteresis in one plane could be determined by calculating the phase difference between the fitted parameterized curves of the average breathing cycles of two directions (Fig. 7). When present, hysteresis was largest in the AP-CC plane (sagittal plane), but was also observed in the other planes (Table 4). A phase shift between the signals did not lead to a measurable hysteresis in four other patients, because the tumor movement was less than 1 mm.

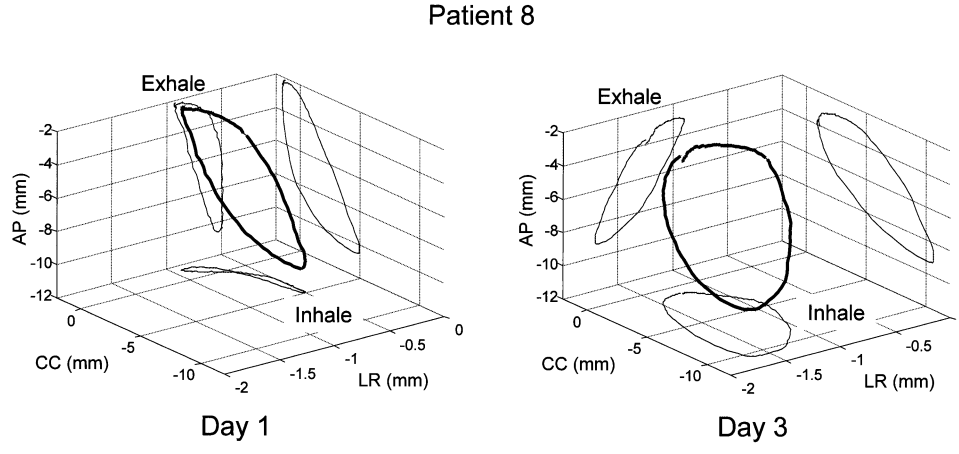

Fig. 5. The 3D trajectory of the tumor of Patient 8: (A) On Day 1, the pattern was similar to that on Day 2 and 4. (B) Day 3. The shape and direction of the motion changed between subsequent days: In the coronal plane on Day 3, hysteresis was present, whereas on Days 1, 2, and 4, this was not the case. In the transaxial (AP-LR) plane, the motion switched from left to right on Days 1, 2, and 4 and to right to left on Day 3.

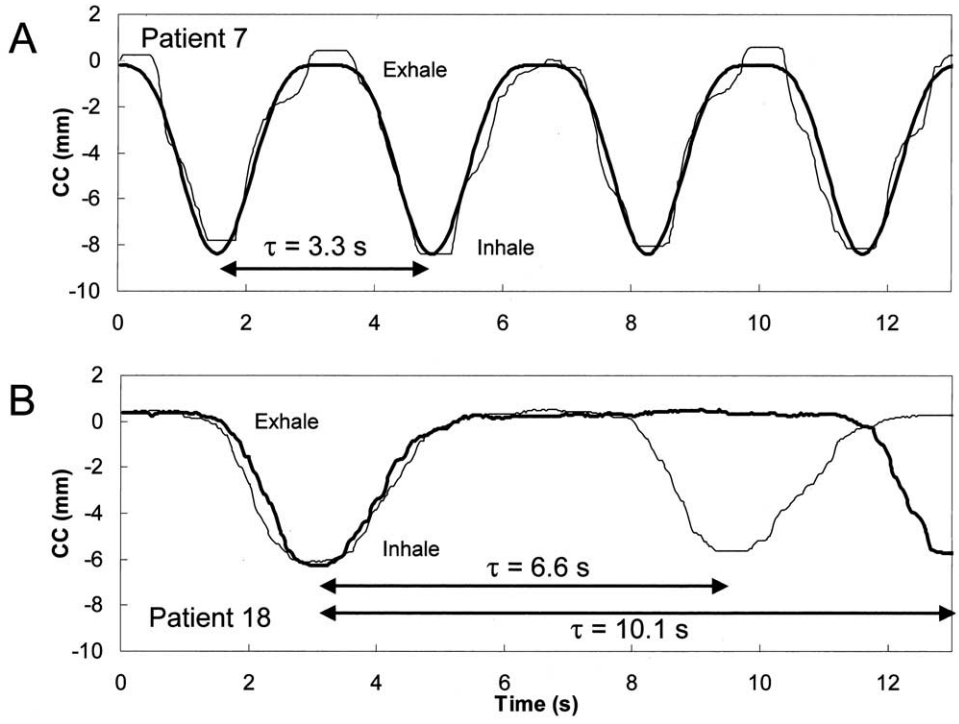

Fig. 6. (A) The time signal of the tumor motion of Patient 7 (CC direction). A curve was fitted through the data with ($\tau = 3.3$ s and $n = 2$. (B) The time signal of the tumor motion of Patient 18, who had a very irregular breathing pattern (CC direction). The thin line represents tumor motion with a period of 6.6 s, whereas later on the period was 10.1 s. The first cycle could be fitted well with $n = 3$; the second cycle was fitted with $n = 9$. Note that the shape of the tumor motion of the longer period is similar to that of the shorter cycle, only the time spent in the exhale position is prolonged in the longer cycle.

Heartbeat

In 7 of the 20 patients, the heartbeat caused a measurable tumor motion (Table 5). When the cardiac frequency was detected in the frequency analysis (Fig. 8A), the amplitude of the tumor motion was measured in the time signal (Fig. 8B). In 2 patients, tumor motion due to the heart was detected in two directions. The tumor was attached to, or near, the aorta in 6 of the 7 patients. The distance of the marker to the cardiac or aortic wall was less than 3 cm in these 6 patients. The motion due to the heartbeat was largest in the LR direction (range: 1–4 mm). In the other directions, the motion was 1–2 mm.

DISCUSSION

The RTRT system is unique in recording the tumor position in all three directions simultaneously at a high sampling rate. This enabled us to detect tumor motion due to the heartbeat, as well as hysteresis. The system measures the position of a gold marker implanted in or near the tumor. In some studies (11, 12, 19, 20, 21), the position of the chest wall or diaphragm is used to monitor breath-holding or to trigger the linear accelerator. However, the position of the tumor can be different from the position of these structures. For example, in the study by Hanley *et al.* (11), the chest wall moved with an amplitude of 2 to 2.5 mm, whereas the diaphragm of the same patients moved 20–38 mm. Minohara *et al.* (20) measured the breathing phase with an ir-LED and a PSD camera. They found a phase difference of about 200 ms between the position of the diaphragm and the respiratory signal from the LED camera system that was placed under the left rib. In other studies, the volume of the inhaled air is used as a measure of the tumor position (6). Although these techniques are useful to determine the inhale or exhale phase of the breathing, the 3D tumor motion and the exact position of the tumor are not measured directly and must be inferred.

During real-time tumor tracking radiotherapy, the shape of the 3D path of the tumor did not change significantly over time. However, its amplitude and position in space varied because of patient shift or "setup" errors, as well as changes in breathing level and intensity. The tumor motion due to breathing is not one-dimensional, as assumed in simulation studies (18, 22), but a combination of movement in all three dimensions, sometimes resulting in hysteresis. However, tumor motion due to breathing is largest in the cranial-caudal direction, especially in unfixed lower-lobe tumors. Tumor motion in the presented patient group agrees with tumor motion found by Ekberg *et al.* (10). In the present study, the amplitude of the movement was different for tumors attached to rigid structures, such as the chest wall or vertebrae. These tumors move only slightly, in agreement

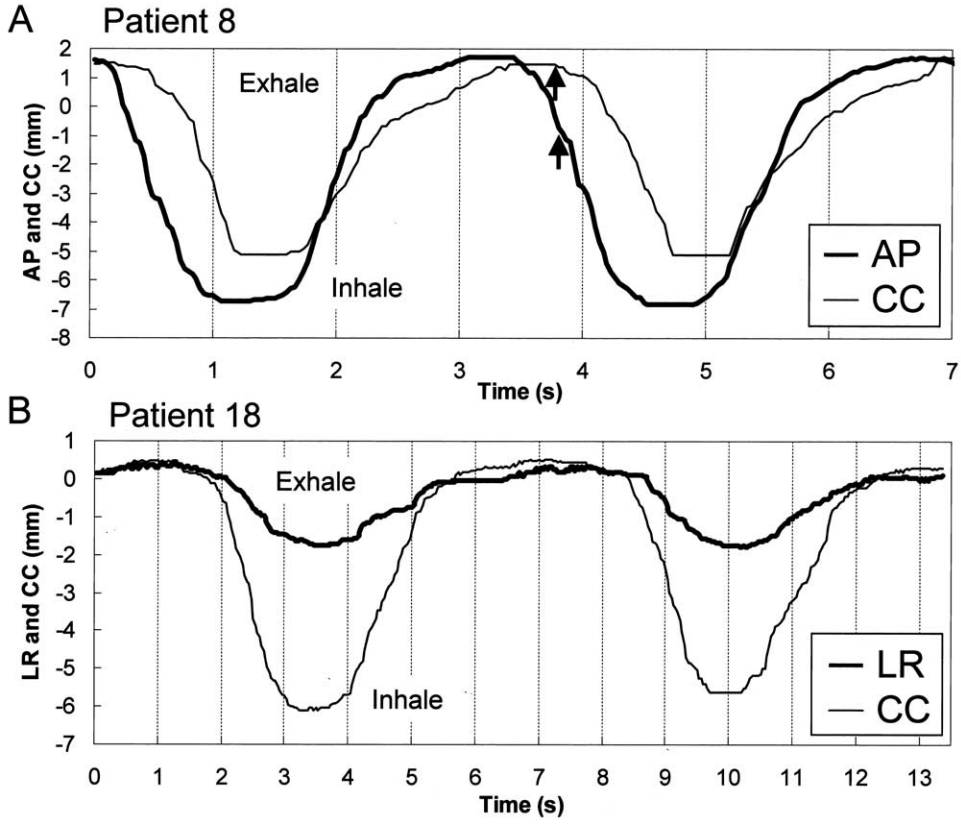

Fig. 7. (A) Time signal of Patient 8 in the AP and CC directions. There was a phase difference ($\Delta\phi$) of 0.5 s between both signals, causing hysteresis. At the arrow, the tumor in the CC direction is still in the exhale position, whereas in the AP direction, inhalation has already started. (B) Time signal of Patient 18 in the AP and CC directions. There was no measurable phase difference between both signals.

with findings by Ross *et al.* (23), who also found that tumors in upper lobes and tumors that were attached to the chest wall moved less than lower-lobe tumors.

Two patients (Patients 8 and 19) showed significant hysteresis. Both tumors were located at a similar position in the lungs, one in the left lung and one in the right (Fig. 4). One of these patients suffered from emphysema with prominent chest breathing. These findings suggest that preexisting lung disease and breathing techniques are important for estimating the amplitude of the tumor motion.

Table 4. The amount of hysteresis (in mm) in three planes

Patient no.	Coronal (mm)	Sagittal (mm)	Transaxial (mm)
1	1.5	1	1
2	1.5	1	
8		5	
9a		2	
9b	2	3	
10	2		
11		1	1.5
12		2	
15		2.5	
19		3	
20	1		

The position of the tumor during the exhale phase of tidal breathing is considered to be the most stable and reproducible position (24). This is assumed in many gated treatment designs, and for the intrafractional period, this was confirmed by our study. However, for some tumors a systematic shift or trend between different beams and/or fractions was observed, particularly in the posterior direction. The variations in the shifts and trends were larger than the variations during one beam and do not differ for the inhalation and exhalation tumor position.

The time trends could be attributed to patient relaxation throughout the treatment (combined with a reduction in amplitude) or to gravity acting on compliant lung tissue shortly after the patient assumes a supine position. A systematic shift could result from changes in muscle tone, a slight shift in patient position, or simply a change in the level at which the patient started breathing. The shifts in exhale position between *subsequent* days can also be caused by the variation in the zero-position of the RTRT treatment. During the setup phase of the treatment, the physician assesses the tumor motion based on two fluoroscopy images. The tumor motion visible on these images is a two-dimensional projection of the real 3D

Table 5. Tumor motion due to heartbeat

Patient no.	Frequency (bpm)	Amplitude (mm)			Lobe	Tumor attached to:	Distance from the cardiac or aortic wall to the marker (mm)
		LR	CC	AP			
2	66	1			Upper	Aorta	30*
5	70	1		1.5	Upper	Bronchus	10
7	62		1		Lower	Aorta	25*
8	60		2		Upper	Free	30
9b	63	2			Upper	Vertebra and aortic arch	15*
11	60	4			Upper	Aorta	27†
15	72		1.5	1	Upper	Free	65*

The discrepancies between the tumor attachment and the distance from the cardiac or the aortic wall to the marker can be explained by:
*The marker was positioned near and not in the tumor.
†The tumor volume was large.
Abbreviations: LR = lateral; CC = cranial-caudal; AP = ventral-dorsal.

motion. It is possible that the zero-position is chosen correctly along one direction, but not necessarily along the other directions. Additionally, it is not possible to put the zero-position at exactly the same position in the breathing cycle each day. Thus, the combination of the placement of zero-position, patient shifts, and changes in breathing level can cause a variation in the order of 1 to 1.5 mm. Improvement in the placement of the zero-position is required for improved accuracy. This can be accomplished by automatically determining the average tumor position relative to the exhale tumor position by means of a short real-time tumor tracking session before the actual treatment. However, interfraction changes in breathing level cannot be monitored with this technique.

To obtain the best treatment efficiency for RTRT treatments, as well as to determine the ideal tumor position for gated or breath-hold radiotherapy or CT, the phase of the breathing cycle representative of the average tumor position must be identified. The tumor motion can be modeled using a periodic but asymmetric function (more time spent at exhale vs. inhale [Eq. 1]). The amount of time the tumor spent in the exhale position differed per patient. The tumor motion was more asymmetric for a patient with a relatively long breathing cycle.

The 3D analysis of the tumor motion revealed also that in some patients, the trajectory of the tumor during inhalation is different from the trajectory during exhalation. This hysteresis can, for example, be induced by the breathing technique, especially when diaphragm and chest breathing are combined asymmetrically. Another possible explanation for hysteresis is the lung's dynamic properties. Because of the elasticity of the lung tissue, the tumor motion may be delayed compared to the motion of the chest wall and/or the diaphragm. It can take a while before the tumor occupies a stationary position (This is reached during the relatively long "rest" periods during the inhalation and especially the exhalation phase). Lung diseases such as emphysema, bullae, or fibrosis can influence the elasticity of lung tissue anisotropically and cause hysteresis. When hysteresis in tumor motion is caused by the dynamic properties of lung tissue, breath-hold scans will not give the representative position of the tumor. During normal breathing, there is hysteresis; during a long breath hold, however, the tumor occupies its stationary position. Hysteresis can seriously affect the accuracy in radiotherapy, which uses the position of skin, diaphragm, or physiologic parameters for respiration gating without considering the respiration phase. During real-time tumor tracking, the tumor may be inside the permitted range for inhalation, but outside for exhalation (Fig. 9). When this occurs in two or three directions, hysteresis can increase the irradiation time considerably. The cause of hysteresis and its effect on treatment accuracy will require further study in the future.

Using discrete Fourier analysis, tumor motion due to heartbeat was detected in 7 of the 20 patients. The amplitude of this motion was 1–4 mm, mostly in the LR direction. Tumor movement with heartbeat was most significant for tumors attached to the aorta. In the fluoroscopy study by Ekberg *et al.* (10), it was observed that for tumors located close to the heart, cardiac movement was a major contributor to tumor motion. In a 20-patient study by Ross *et al.* (23) using an ultra-fast CT scanner, tumor motion of 9 ± 6 mm in the LR and AP directions was measured that was attributed to aortic pulsation, cardiac contraction, and respiration. Neither author distinguished between tumor motion caused by breathing or cardiac motion.

Although real-time tumor tracking using an implanted gold marker resulted in precise information regarding the tumor position, the technique has inherent limitations. The gold marker is not always inserted exactly into the tumor, so the motion measured with the RTRT system may not correspond exactly with the real tumor motion. Measuring marker motion relative to tumor motion during treatment is hampered because of the poor visibility of the tumor in the fluoroscopic images. When the tumor is large, some parts of the tumor may not move as a fixed, rigid structure. Tumor rotation and deformation cannot be detected using a single inserted marker. Furthermore, the presence of the gold

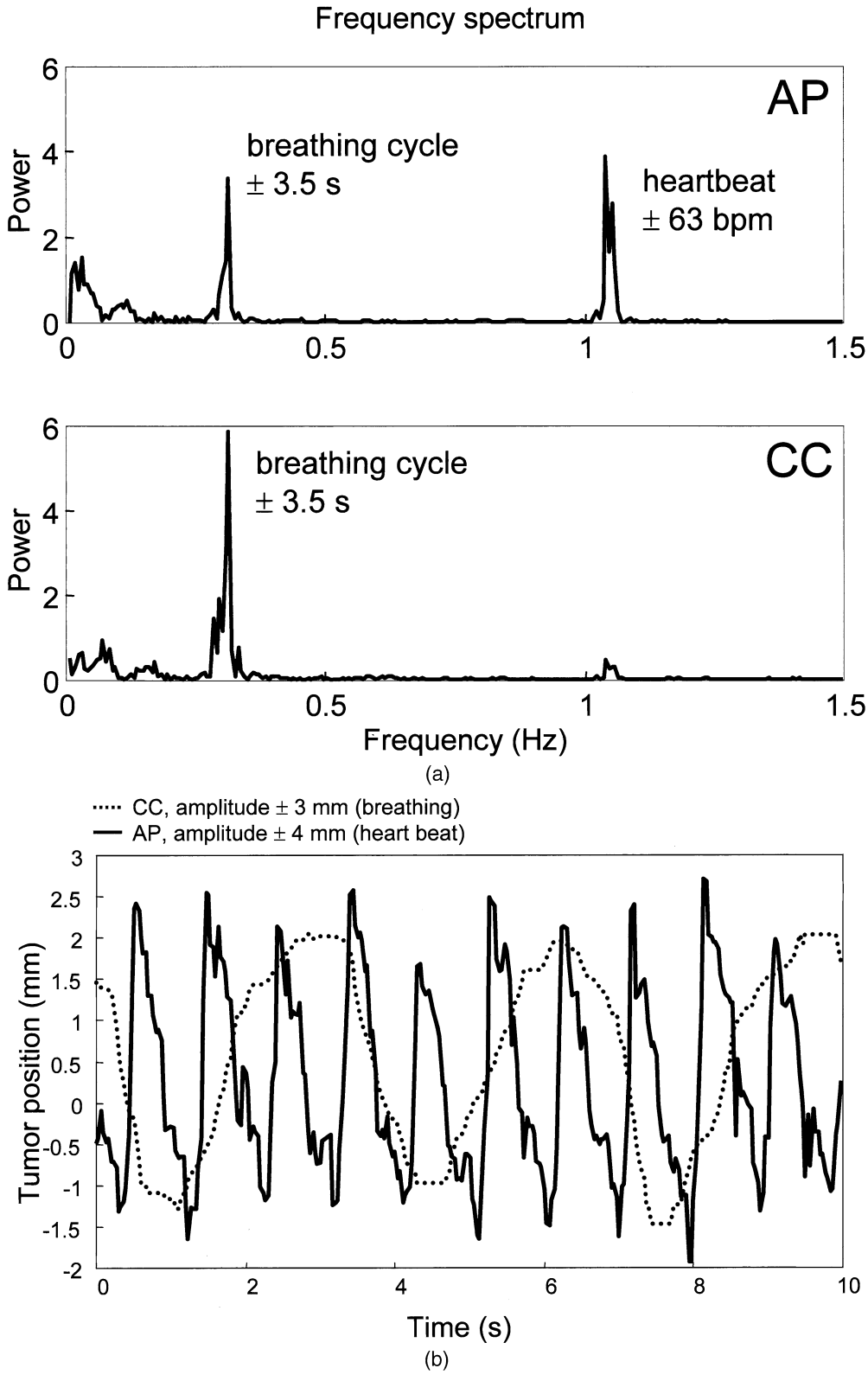

Fig. 8. (a) The frequency spectrum of the LR and CC coordinates of Patient 11. Two frequency peaks are present in the registration, one at 0.3 Hz as a result of breathing and one at 1.05 Hz as a result of the heartbeat. In the CC direction, the power of the heartbeat signal is weak compared to the power of the breathing signal; in the LR direction, the heartbeat has the largest power. (b) The time signals of the LR (solid line) and CC (dotted line) tumor positions. In the LR direction, tumor motion due to heartbeat is visible. In the CC direction, only the breathing is visible.

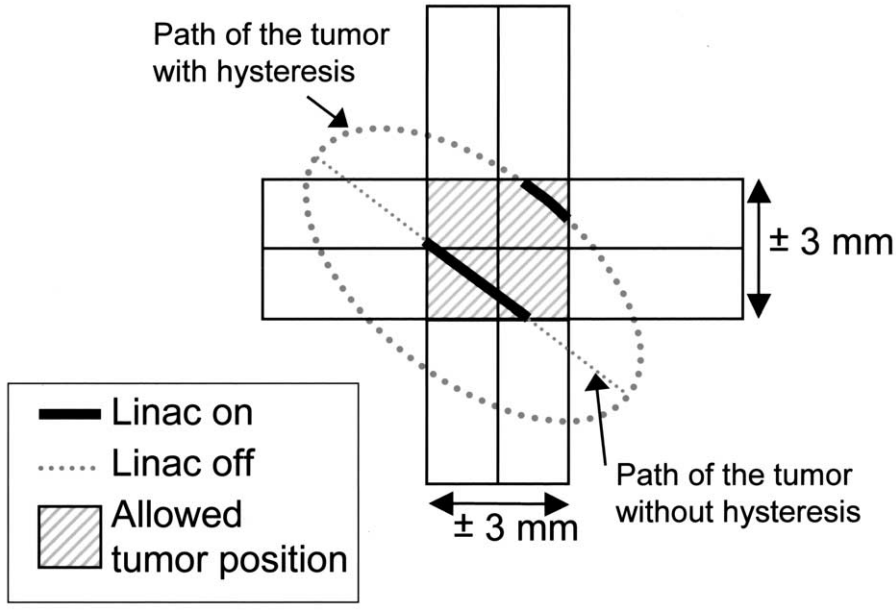

Fig. 9. The path of a moving tumor with and without hysteresis (dotted line) during RTRT treatment. The solid line represents the time that the linear accelerator is irradiating the tumor. When hysteresis is present, the tumor is irradiated during only about 10% of the treatment time; when there is no hysteresis, the tumor is irradiated about 30% of treatment time.

marker (relatively heavy compared to the lighter lung tissue) may distort the tumor motion or result in hysteresis. Migration of the internal marker was not studied in lung cancer, but was small (on the same order as CT accuracy) in prostate and liver cancer studies (25). Experiments have already begun involving implantation of three markers to measure rotation and tumor shrinkage. Breath-hold and repeat CTs will be made to assess marker migration and tumor motion relative to marker motion.

CONCLUSION

In conclusion, the RTRT system has been used to measure tumor position in all three orthogonal directions simultaneously, at a high sampling rate that enabled the detection of tumor motion due to heartbeat, as well as hysteresis. Tumor motion and hysteresis could be modeled with an asymmetric trigonometric function. Tumor motion due to breathing was greatest in the cranial-caudal direction for lower-lobe unfixed tumors.

REFERENCES

1. Armstrong J, Raben A, Zelefsky M, *et al*. Promising survival with three-dimensional conformal radiation therapy for non-small cell lung cancer. *Radiother Oncol* 1997;44:17–22.
2. Belderbos JSA, De Jaeger K, Baas P, Lebesque JV. Dose escalation in NSCLC using three dimensional conformal radiotherapy (3DCRT). *Lung Cancer* 2000;29(Suppl. 1)(545):161.
3. Hayman JA, Martel MK, Ten Haken RK, *et al*. Dose escalation in non-small-cell lung cancer using three-dimensional conformal radiation therapy: Update of a Phase I trial. *J Clin Oncol* 2001;19:127–136.
4. Mehta M, Scrimger R, Mackie R, *et al*. A new approach to dose escalation in non-small cell lung cancer. *Int J Radiat Oncol Biol Phys* 2001;49:23–33.
5. Robertson JM, Ten Haken RK, Hazuka MB, *et al*. Dose escalation for non-small cell lung cancer using conformal radiation therapy. *Int J Radiat Oncol Biol Phys* 1997;37:1079–1085.
6. Wong JW, Sharpe MB, Jaffray DA, *et al*. The use of active breathing control (ABC) to reduce margin for breathing motion. *Int J Radiat Oncol Biol Phys* 1999;44:911–919.
7. Bel A, Bartelink H, Vijlbrief RE, *et al*. Transfer errors of planning CT to simulator: A possible source of setup inaccuracies? *Radiother Oncol* 1994;31:176–180.
8. de Boer HC, van Sornsen de Koste JR, Senan S, *et al*. Analysis and reduction of 3D systematic and random setup errors during the simulation and treatment of lung cancer patients with CT-based external beam radiotherapy dose planning. *Int J Radiat Oncol Biol Phys* 2001;49:857–868.
9. Balter JM, Ten Haken RK, Lawrence TS, *et al*. Uncertainties in CT-based radiation therapy treatment planning associated with patient breathing. *Int J Radiat Oncol Biol Phys* 1996;36: 167–174.
10. Ekberg L, Holmberg O, Wittgren L, *et al*. What margins should be added to the clinical target volume in radiotherapy treatment planning for lung cancer? *Radiother Oncol* 1998;48:71–77.
11. Hanley J, Debois MM, Mah D, *et al*. Deep inspiration breath-hold technique for lung tumors: The potential value of target immobilization and reduced lung density in dose escalation. *Int J Radiat Oncol Biol Phys* 1999;45:603–611.
12. Kubo HD, Len PM, Minohara S, *et al*. Breathing-synchronized radiotherapy program at the University of California Davis Cancer Center. *Med Phys* 2000;27:346–353.
13. Kubo HD, Len PM, Minohara S, *et al*. Breathing-synchronized radiotherapy program at the University of California Davis Cancer Center. *Med Phys* 2000;27:346–353.

14. Shirato H, Shimizu S, Shimizu T, *et al*. Real-time tumour-tracking radiotherapy. *Lancet* 1999;353:1331–1332.
15. Shirato H, Shimizu S, Kunieda T, *et al*. Physical aspects of a real-time tumor-tracking system for gated radiotherapy. *Int J Radiat Oncol Biol Phys* 2000;48:1187–1195.
16. Shirato H, Shimizu S, Kitamura K, *et al*. Four-dimensional treatment planning and fluoroscopic real-time tumor tracking radiotherapy for moving tumor. *Int J Radiat Oncol Biol Phys* 2000;48:435–442.
17. Shimizu S, Shirato H, Kagei K, *et al*. Impact of respiratory movement on the computed tomographic images of small lung tumors in three-dimensional (3D) radiotherapy. *Int J Radiat Oncol Biol Phys* 2000;46:1127–1133.
18. Lujan AE, Larsen EW, Balter JM, *et al*. A method for incorporating organ motion due to breathing into 3D dose calculations. *Med Phys* 1999;26:715–720.
19. Rosenzweig KE, Hanley J, Mah D, *et al*. The deep inspiration breath-hold technique in the treatment of inoperable non-small-cell lung cancer. *Int J Radiat Oncol Biol Phys* 2000;48: 81–87.
20. Minohara S, Kanai T, Endo M, *et al*. Respiratory gated irradiation system for heavy-ion radiotherapy. *Int J Radiat Oncol Biol Phys* 2000;47:1097–1103.
21. Mah D, Hanley J, Rosenzweig KE, *et al*. Technical aspects of the deep inspiration breath-hold technique in the treatment of thoracic cancer. *Int J Radiat Oncol Biol Phys* 2000;48:1175–1185.
22. Engelsman M, Damen EMF, De Jaeger K, *et al*. The effect of breathing and set-up errors on the cumulative dose to a lung tumor. *Radiother Oncol* 2001;60:95–105.
23. Ross CS, Hussey DH, Pennington EC, *et al*. Analysis of movement of intrathoracic neoplasms using ultrafast computerized tomography. *Int J Radiat Oncol Biol Phys* 1990;18: 671–677.
24. Balter JM, Lam KL, McGinn CJ, *et al*. Improvement of CT-based treatment-planning models of abdominal targets using static exhale imaging. *Int J Radiat Oncol Biol Phys* 1998;41:939–943.
25. Kitamura K, Shirato H, Shimizu S. Migration of the internal fiducial gold marker implanted into prostate and liver treated with real-time tumor-tracking radiation treatment (RTRT). *Int J Radiat Oncol Biol Phys* 2000;48(3S):343–344.